

Research Paper

Different fatigue behavior between tension-tension and tension-compression of carbon nanotubes reinforced 7055 Al composite with bimodal structure



S. Bi ^{a, b}, Z.Y. Liu ^{a, *}, B.L. Xiao ^a, P. Xue ^a, D. Wang ^a, Q.Z. Wang ^a, D.R. Ni ^a, Z.Y. Ma ^a

^a Shi-changxu Innovation Center for Advanced Materials, Institute of Metal Research, Chinese Academy of Sciences, 72 Wenhua Road, Shenyang, 110016, China

^b University of Science and Technology of China, School of Material Science and Engineering, 72 Wenhua Road, Shenyang, 110016, China

ARTICLE INFO

Article history:

Received 18 April 2021

Received in revised form

3 August 2021

Accepted 14 August 2021

Available online 19 August 2021

Keywords:

Carbon nanotube

Aluminum matrix composites

Bimodal structure

Fatigue

Tension-tension

Tension-compression

ABSTRACT

Understanding the fatigue behavior of Carbon nanotube (CNT) reinforced Al composites (CNT/Al) was of critical importance, for their further application in the aerospace industry. Although CNT could improve the fatigue performance, the fatigue behavior of CNT/Al composites with different structure (e.g. bimodal structure) under different fatigue conditions was still in lacking. In this study, the tension-tension/tension-compression fatigue behaviors of bimodal structure CNT/7055Al composites consisting of ultra-fine grain (UFG) zones rich of CNTs and coarse grain (CG) bands free of CNTs, were investigated and the corresponding damage mechanisms were analyzed. Results indicated that dislocation cells, tangles and subgrains were observed in the CGs, while no obvious dislocation configuration was detected in the UFGs after 10^7 fatigue cycles. Under the tension-tension fatigue condition, the fatigue strength of the composites was increased from 350 MPa to 400 MPa by load transfer effect of CNTs at 10^7 cycles. However, CNTs failed to improve the fatigue strength under the tension-compression fatigue condition due to the failure of the UFG zones rich of CNTs resulting from the high stress amplitude. It was found that strain localization in the CGs was the principal damage mechanism of CNT/7055Al composites.

© 2021 Elsevier Ltd. All rights reserved.

1. Introduction

Owing to the outstanding properties of carbon nanotubes (CNTs) (strength of ~30 GPa and Young's modulus of ~1 TPa), CNT reinforced aluminium matrix (CNT/Al) composites have attracted great attention since the past decade [1–5]. Possessing high strength, high stiffness and low density, CNT/Al composites have broad application prospects in the fields of aerospace and automobile [6–9]. However, the early work on CNT/Al composites only focused on the strength and stiffness [10–15], ductility [16–19], hot deformation [1,20] and wearability [21], while little attention had been paid to the fatigue performance which affected the dynamic service safety. The understanding of fatigue behavior of the CNT/Al composites can provide a basis for the dynamic performance design of CNT/Al composites and a reference for the reliable service of CNT/Al composites in the future.

Actually, a number of studies have been conducted on the fatigue behavior of particle reinforced aluminum matrix composites (AMCs) and demonstrated that the AMCs exhibited better high-cycle fatigue performance than the unreinforced aluminum alloys [22–26]. Chawla et al. [22] and Llorca et al. [27] found that the load transfer effect of the reinforcements reduced the average stress level in the matrix, and retarded the crack nucleation. Myriounis et al. [28] found that the ceramic particles would hinder fatigue crack propagation and reduce the crack propagation rate. In general, the fatigue strength (FS) of the AMCs increased with the increase of reinforcement contents [23,24,27,29]. In addition, the particle size had a significant influence on the fatigue properties of the AMCs [30,31]. Large particles would cause crack initiation, which was disadvantageous to the fatigue performance. By comparison, small particles could hinder dislocation motion, reduce strain localization and improve the fatigue performance.

However, only limited numbers of studies have been conducted on the fatigue behavior of CNT/Al composites. Liao et al. [32] reported the tension-tension fatigue behavior of CNT/Al composites under a stress ratio of 0.1, and found that CNTs significantly

* Corresponding author.
E-mail address: zylu@imr.ac.cn (Z.Y. Liu).

enhanced the number of load cycles to failure of the composites by crack-bridging and pulling-out mechanisms. Shin et al. [33] found that the incompatibility between CNTs and Al matrix generated by cyclic deformation resulted in CNT pulling-out. The pulled-out CNTs reduced the energy of crack propagation and acted as bridges to prevent crack further propagation. As a result, the FS of the 4 vol% CNT/2024Al composite under the severe condition (stress ratio of -0.5) reached 550 MPa and the fatigue ratio reached 0.78. However, the corresponding microstructure evolution during fatigue was still lacking, and the fatigue behavior of the composites under more severe conditions (such as the stress ratio of -1) was not reported.

As well known, crack initiation life comprised over 90% of the total fatigue life [34]. An in-depth understanding of damage mechanism can help to delay crack initiation and improve the fatigue performance of CNT/Al composites. Although the previous studies have reported the reinforcing effect of CNTs during fatigue, the effect of CNTs under more stringent condition is still necessary to study.

Recently, heterogeneous structure (e.g. bimodal structure) was demonstrated to be an effective way to improve the strength-ductility as compared to homogeneous structure for CNT/Al composites [11,19,35,36]. Ma et al. [36] optimized the CG structure in bimodal CNT/2009Al composites via hot extrusion process and enhanced the ductility by 60%. Liu et al. [35] enhanced the ductility from 2% to 4.5% with nearly no strength loss via optimizing proportion of CGs and UFGs in CNT/Al–Cu–Mg composites. Bimodal structure design has become an important trend for toughening CNT/Al composites. However, some previous investigations on alloys indicated that the relatively weak zones in the heterogeneous materials could be the preferential sites for fatigue damage [37,38], which makes the fatigue behavior of heterogeneous materials quite different from the homogeneous composites. Whether the bimodal structure would affect the fatigue damage behavior of CNT/Al composites was still to be investigated.

Our previous investigation demonstrated that using 7xxx series Al alloy as the matrix could lead to higher strength and deformation ability [6,39,40] as compared with those using pure Al, 5xxxAl or 6xxxAl series alloy. Further, bimodal structure could be in-situ formed in the CNT/7055Al composites [7,20], which made CNT/7055Al composites the ideal model materials for fatigue investigation.

In the present study, the high-cycle fatigue behaviors of CNT/7055Al composites under the stress ratios of 0.1 and -1 were respectively investigated. The microstructure, surface morphology and fractograph after fatigue deformation were analyzed. The objective of this study is: (i) to clarify the damage mechanism of CNT/7xxx Al composites with bimodal structure and (ii) to explicate the effect of bimodal structure and CNTs on fatigue behavior under different cyclic loading condition.

2. Experimental

The 7055Al alloy and CNT/7055Al composite were fabricated by ball-milling and powder metallurgy route. An attritor was utilized to disperse 2 vol% multi-walled CNTs (about 15 nm in diameter, 2–5 μm in length, and supplied from Cnano Technology Ltd., Jiangsu, China) in 7055Al alloy powders (Al-8.1 wt% Zn-2.2 wt% Mg-2.2 wt% Cu, about 10 μm in diameter). Milling was conducted at 400 rpm for 6 h with a ball-to-powder ratio of 15:1 in a purity argon atmosphere, as described in our previous reports [39,40]. 1.6 wt% stearic acid was added as the process control agent to prevent excessive cold welding of powders.

The milled powders were cold-compacted into a cylinder die and then hot-pressed at 500 $^{\circ}\text{C}$ for 1.5 h to form a cylinder billet

($\Phi 75\text{ mm} \times 80\text{ mm}$). The as-pressed billet was then hot extruded at 420 $^{\circ}\text{C}$ into bar with an extrusion ratio of 16:1. The extruded composite samples were solution treated at 470 $^{\circ}\text{C}$ for 1 h to dissolve coarse second-phases, and then quenched into water. Aging of the solution-treated samples were carried out at 120 $^{\circ}\text{C}$ for 24 h. For comparison, 7055Al alloy samples were prepared under the same process and subjected to the same heat treatment conditions.

Optical microscopy (OM, Leica DMi8M) and transmission electron microscopy (TEM, Tecnai G2 20, Talos F200X) were employed to observe the microstructure. TEM specimens were cut by electrical discharge machining, ground to a thickness of 60 μm , punched to disks with a diameter of 3 mm, then dimpled to a minimum thickness of 20 μm and finally ion-beam thinned by a Gatan Model 691 ion milling system. Scanning electron microscopy (SEM, FEI-Apreo) was used to characterize the surface morphology and fractograph. In order to evaluate the stress suffered on the CNTs after fatigue, Raman spectroscopic examination was performed on the fatigue specimens using a micro-Raman spectroscope (Jobin Yvon HR800, excited by 532 nm He–Ne laser with laser size of $\sim 1\ \mu\text{m}^2$) in the spectral range from 1450 to 1800 cm^{-1} .

Tensile specimens with a gauge diameter of 5 mm and length of 25 mm, and fatigue specimens with a gauge diameter of 6 mm and length of 10 mm were respectively machined along the extrusion direction. Tensile test was carried out on an Instron 5982 tester at a strain rate of $1 \times 10^{-3}\ \text{s}^{-1}$ at room temperature. High-cycle fatigue test was performed on an Instron 8801 tester with servo-hydraulic system under the load-controlled mode at a frequency of 20 Hz at room temperature. The specimens were axially fatigued at stress ratios of $R = 0.1$ and -1 ($R = \sigma_{\min}/\sigma_{\max}$, σ_{\min} and σ_{\max} are minimum and maximum stresses, respectively). The FS was determined at about 10^7 cycles according to the most of the fatigue limit of Metals [33]. In order to observe the surface morphology of specimens after fatigue, plate specimens with gauge section of 5 mm \times 3 mm \times 2.5 mm were machined parallel to the extrusion direction. The specimen surfaces were mechanically polished followed by electropolishing. The electropolishing was performed in a solution of 30 mL HF + 11 g H_3BO_3 + 970 mL H_2O at room temperature and a voltage of 20 V.

3. Results

3.1. Microstructure before fatigue

Fig. 1 shows the microstructure of the CNT/7055Al composite. The OM image in Fig. 1a indicates that the composite had a pronounced inhomogeneous structure. The TEM image in Fig. 1b demonstrates that the composite consisted of coarse grain (CG) band and ultra-fine grain (UFG) zone. The CG band with a width of $\sim 1\ \mu\text{m}$ consisted of fine grains with grain sizes about 1 μm , where no CNTs could be observed (Fig. 1b). The grain size of the UFGs was about 200–300 nm, and CNTs with a length of about 100 nm were uniformly distributed in the UFG zone (Fig. 1c). Further, tube structure of CNT was well retained and CNT–Al interface was well bonded (Fig. 1d). These above indicate an obvious bimodal structure formed for the CNT/7055Al composite. This bimodal structure could be due to the decrease of solidus temperature induced by high alloying elements, which led to the formation of some liquid phases during hot pressing. And these liquid phases formed during hot pressing changed into the CG bands free of CNTs after solidification [7].

3.2. Tensile and fatigue properties

Tensile properties of the 7055Al and CNT/7055Al composites are listed in Table 1. As shown, the 2 vol% CNT/7055Al composite

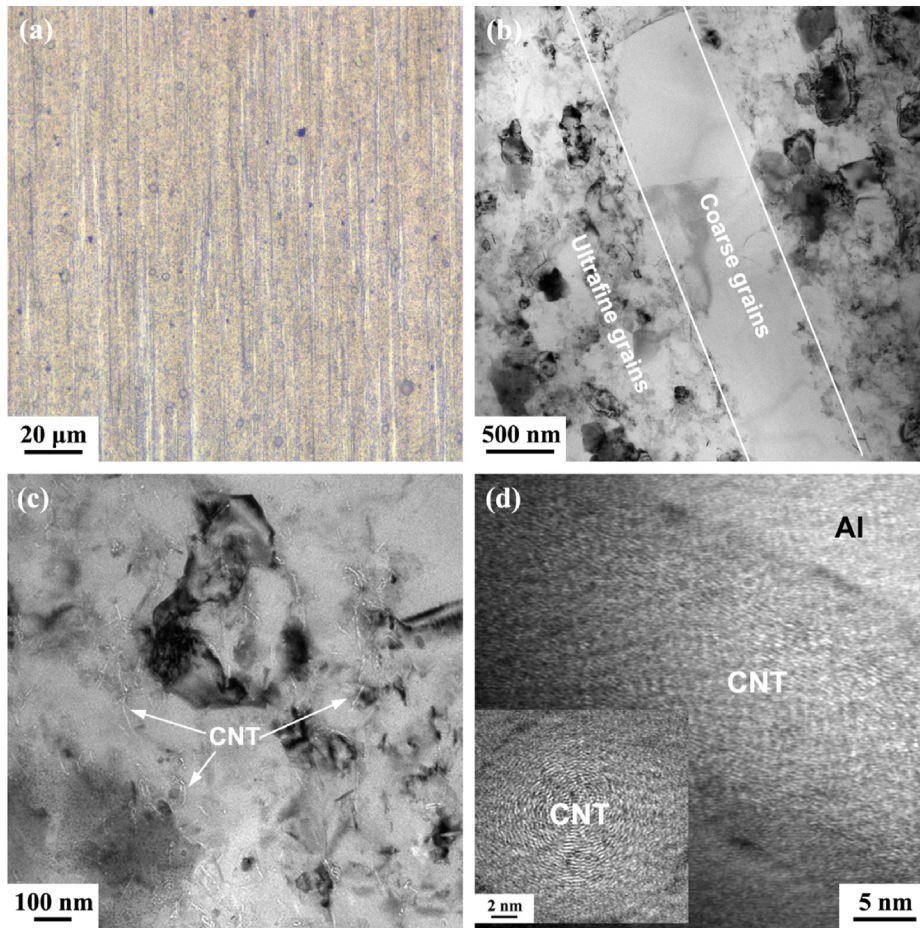


Fig. 1. (a) Typical OM image and (b) TEM image of CNT/7055Al composite, and TEM images showing (c) CNT distribution and (d) CNT structure in the UFG zone. (A colour version of this figure can be viewed online.)

exhibited a high tensile strength of 780 MPa, which is about 80 MPa higher than the unreinforced alloy. As reported in our previous study [7], fine grain, load transfer and Orowan strengthening were the main strengthening mechanisms of the CNT/7055Al composites. It has been reported that the bimodal structure could improve the strength-ductility of CNT/Al composites via blunting crack propagation and relaxing the stress concentration in the UFG zone [35]. However, the elongations of either the matrix or composites were still relatively low, because the UFG had a weak dislocation capacity and the CG content was not high enough for toughening [35].

Fig. 2 shows the maximum stress σ_{max} as a function of the number of cycles-to-failure (N_f) under $R = 0.1$ and -1 , and the N_f data are listed in Table 2. Under the tension-tension condition ($R = 0.1$), the FS of the composite and the alloy were 400 MPa and 350 MPa, respectively, indicating that the addition of CNTs enhanced the FS of the 7055Al alloy. However, under the tension-compression condition ($R = -1$), the FS of the composite and the alloy were both 300 MPa, suggesting the insignificant strengthening of CNTs under the tension-compression fatigue.

Table 1
Tensile properties of the 7055Al and CNT/7055Al composites.

CNT contents	YS/MPa	UTS/MPa	EI/%
0	657 ± 11	700 ± 8	2.8 ± 0.6
2 vol%	712 ± 2	780 ± 3	1.5 ± 0.2

YS: Yield strength; UTS: Ultimate tensile strength.

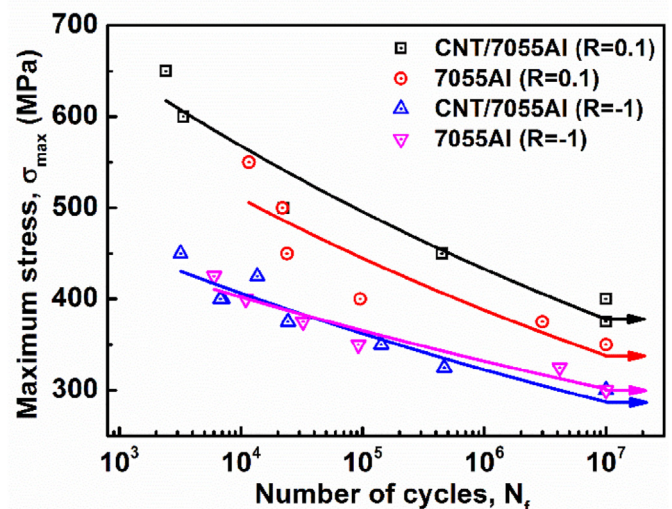


Fig. 2. The maximum stress versus cycle number ($S-N$) curves of the unreinforced 7055Al and CNT/7055Al composites. (A colour version of this figure can be viewed online.)

3.3. Fatigue behavior of CNT/7055Al composites

Fatigue lives for the CNT/7055Al and matrix alloy were evaluated using the Basquin equation in which the nominal strain was in the elastic range as represented by:

Table 2
The failure cycle number (N_f) of the specimens under different fatigue conditions.

Specimens	R	Materials	σ_{max} (MPa)	N_f	Specimens	R	Materials	σ_{max} (MPa)	N_f
1#	0.1	CNT/7055Al	650	2417	14#	-1	CNT/7055Al	425	13,623
2#	0.1	CNT/7055Al	600	3358	15#	-1	CNT/7055Al	400	7041
3#	0.1	CNT/7055Al	500	22,547	16#	-1	CNT/7055Al	400	6794
4#	0.1	CNT/7055Al	450	448,148	17#	-1	CNT/7055Al	375	24,353
5#	0.1	CNT/7055Al	400	10,000,000	18#	-1	CNT/7055Al	350	142,180
6#	0.1	CNT/7055Al	375	10,000,000	19#	-1	CNT/7055Al	325	467,889
7#	0.1	7055Al	550	11,624	20#	-1	CNT/7055Al	300	10,000,000
8#	0.1	7055Al	500	21,927	21#	-1	7055Al	425	6020
9#	0.1	7055Al	450	23,906	22#	-1	7055Al	400	10,951
10#	0.1	7055Al	400	95,585	23#	-1	7055Al	375	32,305
11#	0.1	7055Al	375	2,991,053	24#	-1	7055Al	350	92,186
12#	0.1	7055Al	300	10,000,000	25#	-1	7055Al	325	4,167,280
13#	-1	CNT/7055Al	450	3190	26#	-1	7055Al	300	10,000,000

$$\sigma_a = \frac{\Delta \varepsilon_e E}{2} = \sigma'_f (2N_f)^{-b} \quad (1)$$

where σ_a is the alternating stress amplitude, E is young's modulus, σ'_f is the FS and approximately equal to the true fracture stress σ_f , and b is the fatigue strength exponent ranging from -0.05 to -0.12 for metals. The calculated values of b were listed in Table 3. Under the tension-tension fatigue ($R = 0.1$), the value of $-b$ for the matrix alloy and composite were quite similar. However, under the tension-compression fatigue ($R = -1$), the value of $-b$ for the composite was a little larger than that of the matrix alloy. In general, a smaller value of $-b$ showed a longer cycles-to-failure.

Fig. 3 shows the typical stress-displacement hysteresis loop of the first, mid-life and last cycles for CNT/7055Al composites under $R = 0.1$ and $R = -1$. Under $R = 0.1$, it is evident that the displacement shift occurred as the fatigue cycle progressed. From the first cycle to the mid-life cycle, the composites experienced relatively large elastic displacement. As the fatigue cycle exceeded the mid-life cycle, the elastic displacement change was small. Similar results were also reported in the fatigue deformation of CNT/2024Al composite [33], in which the shifted elastic displacement resulting from the number of cycles was attributed to the cyclic hardening response. Under $R = -1$, from the first cycle to the mid-life cycle, the elastic displacement largely shifted towards the compression direction. As the fatigue cycle increased, the elastic displacement shifted towards the tension direction. This might be related to the tension-compression deformation.

The area of the hysteresis loop was hysteresis energy, which could reveal the degree of plastic deformation of the composite and matrix alloy. Under both $R = 0.1$ and $R = -1$ conditions, the hysteresis loops were small, implying that the elastic deformation dominated the whole high-cycle fatigue of CNT/7055Al composites and only a little plastic deformation occurred. This could be understood because the applied stress under high cycle fatigue was much lower than the YS of the materials, and most of the zones for the materials were still at the elastic stage.

3.4. Observation of fatigue fractograph

Fig. 4a and b shows the typical macro-fractograph of the CNT/7055Al specimens under $R = 0.1$ and $R = -1$, respectively. Three

Table 3
The value of $-b$ for matrix alloy and composites under different fatigue conditions.

	Materials	$R = 0.1$	$R = -1$
$-b$	7055Al	0.05961	0.04165
	CNT/7055Al	0.05891	0.05018

typical zones including crack initiation, crack propagation and final fracture zones were both clearly observed under two different loading conditions. Obviously, the crack propagation zone showing a typical "shellfish" pattern accounted for a large proportion of the whole fracture surface. This was believed to be the effect of the bimodal structure and CNTs on the crack propagation [33,41,42]. It was reported that CG bands could blunt crack tip and hinder crack propagation during tensile deformation [35]. Further, Liao et al. [32] pointed out that CNTs could decrease the crack propagation rate by crack bridging effect.

The magnified images of the crack initiation zones under $R = 0.1$ and $R = -1$ are shown in Fig. 4c and d, respectively. It can be seen that the fatigue cracks both initiated from the surfaces of the specimens under the two different conditions. Although inclusions, holes or agglomeration of reinforcements were usually reported to be the main locations for fatigue crack initiation in AMCs [34], the fatigue cracks in our CNT/7055Al composites did not initiate at second phases. This was because the second phases in the CNT/7055Al composites were relatively small (less than $2 \mu\text{m}$) [6].

Fig. 5 shows the fractograph of the CNT/7055Al specimens under $\sigma_{max} = 500 \text{ MPa}$ and $R = 0.1$. Under low magnification (Fig. 5a and c), both shallow and fine dimples were observed in the crack propagation and final fracture zones, where the dimple sizes were smaller than 200 nm . Also, many wide tear ridges (marked by yellow arrows) were detected. This was the typical morphology of the CG band in the bimodal CNT/2009Al composite after fracture [35]. The formation of the tear ridges indicated the interfaces between CG bands and UFG zones were well bonded, and the CG bands had good deformability during the crack propagation stage. Under high-magnification (Fig. 5b and d), pulled-out CNTs (marked by black arrows) could be observed at the bottom of the dimples.

Fig. 6 shows the fractograph of the CNT/7055Al specimens under $\sigma_{max} = 350 \text{ MPa}$ and $R = -1$. Under low magnification, several tear ridges formed by CG bands were observed in the crack propagation zone (Fig. 6a). The final fracture zone was relatively flat, and no tear ridge was observed (Fig. 6c). Under high magnification, small dimples $\sim 100 \text{ nm}$ were detected in the crack propagation zone (Fig. 6b). The final fracture zone was flat, and the dimples were not obvious (Fig. 6d). In addition, no significant pulled-out CNTs were observed in either zone, which was quite different from that under tension-tension fatigue.

3.5. Microstructure evolution after fatigue

Fig. 7 shows the microstructure of the CNT/7055Al specimen after fatigue under $\sigma_{max} = 600 \text{ MPa}$ and $R = 0.1$. Under high stress tension-tension fatigue, a few dislocations were detected at the CG interior (Fig. 7a), and some dislocations piled up at the boundaries

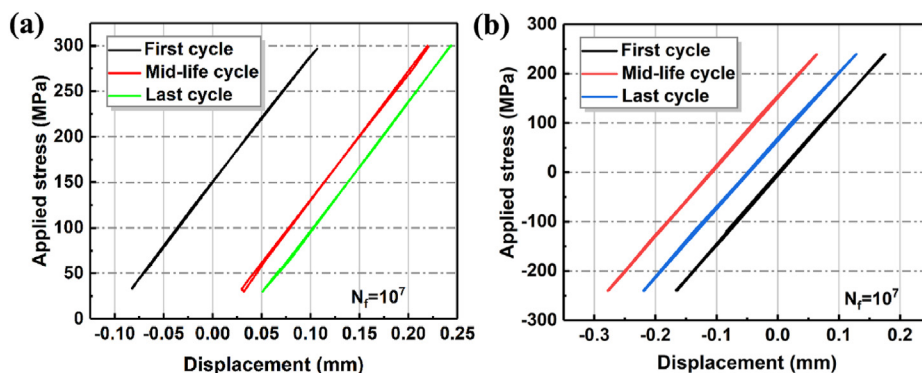


Fig. 3. Typical stress-displacement hysteresis loop of the first, mid-life and last cycles for CNT/7055Al composites under (a) $\sigma_{max} = 400$ MPa, $R = 0.1$ and (b) $\sigma_{max} = 300$ MPa, $R = -1$. (A colour version of this figure can be viewed online.)

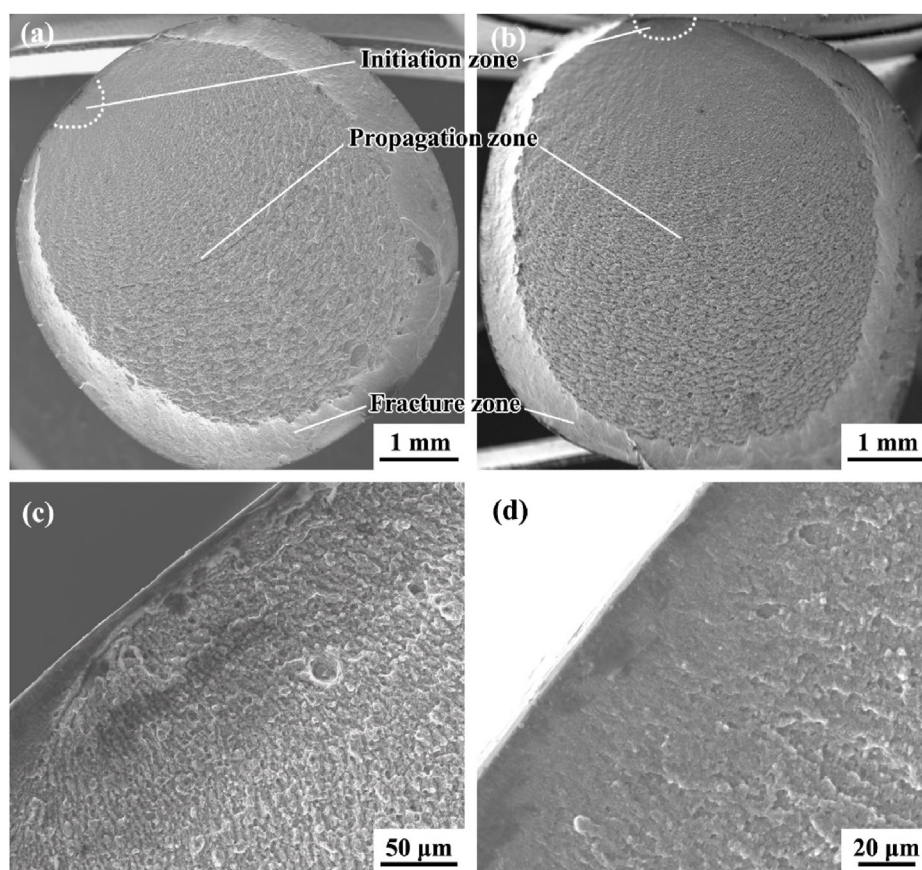


Fig. 4. Fatigue fractograph of CNT/7055Al specimens tested under (a, c) $\sigma_{max} = 600$ MPa, $R = 0.1$ and (b, d) $\sigma_{max} = 450$ MPa, $R = -1$.

between CG and UFG zones, as marked by the yellow rectangles. These piled up dislocations might attribute to the high strain mismatch between CG and UFG zones [43]. No obvious dislocations were observed in the UFGs, and the UFGs did not coarsen during fatigue as compared to the microstructure before fatigue (Fig. 7b). Furthermore, the morphology as well as distribution of CNTs did not change after fatigue (Fig. 7c).

In general, grain coarsening was considered to be the main fatigue damage pattern in nano-grain or UFG materials, e.g. Mughrabi et al. [44] and Malekjani et al. [45] reported that grain coarsening would promote dislocation slip and reduce fatigue properties. In present study, the grains in the CG bands or UFG zones did not

coarsen during cycle deformation, which was due to the strong pinning effect of the CNTs [46].

Fig. 8 shows the microstructure of the CNT/7055Al specimen after 10^7 cycles under $\sigma_{max} = 400$ MPa and $R = 0.1$. Under low stress tension-tension fatigue, a high density of dislocations and dislocation cells were observed in the CG bands (Fig. 8a). The interactions between the precipitates and dislocations were also observed, as shown in the zone A in Fig. 8a. These precipitates could hinder dislocation slip and reduce strain localization during the fatigue of CNT/7055Al composite. Furthermore, sub-grains and dislocation walls were formed inside the CGs, as shown in the zone B in Fig. 8a. The UFG interiors were clean and no obvious dislocation

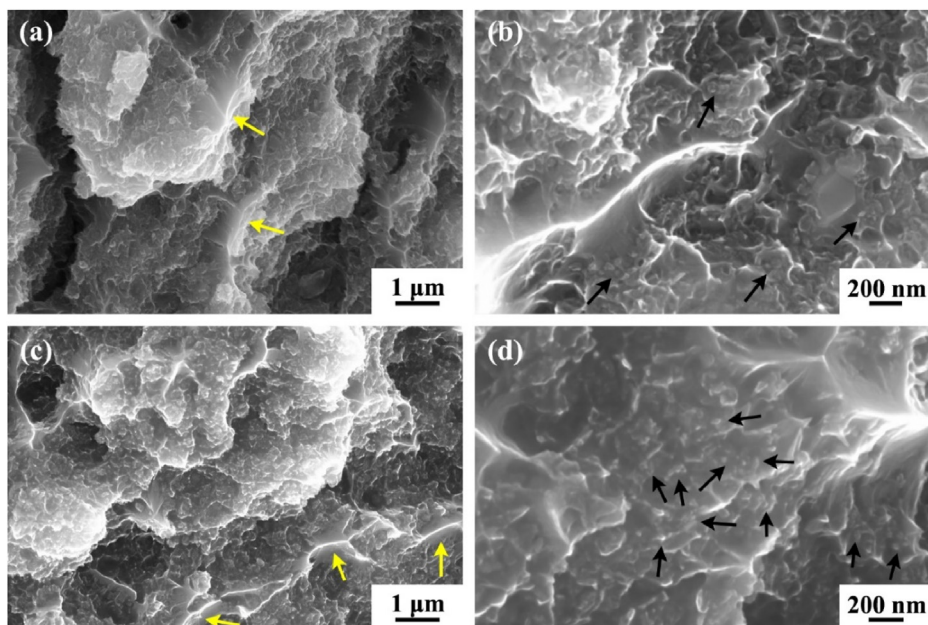


Fig. 5. Fractograph of CNT/7055Al specimens tested under $\sigma_{max} = 500$ MPa, $R = 0.1$: (a, b) crack propagation zone; (c, d) final fracture zone (Yellow and black arrows denote tear ridges and CNTs, respectively). (A colour version of this figure can be viewed online.)

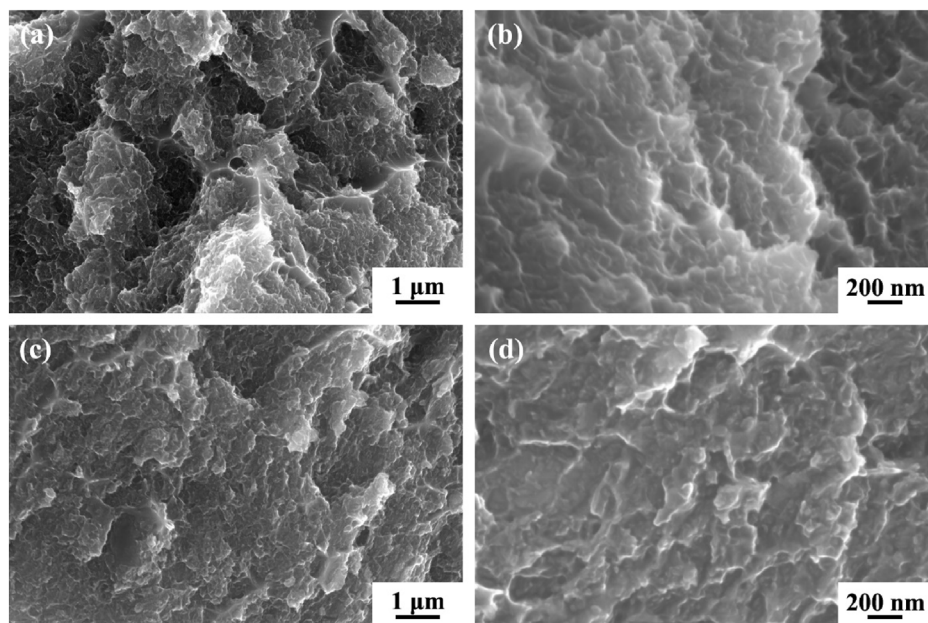


Fig. 6. Fractograph of CNT/7055Al specimens tested under $\sigma_{max} = 350$ MPa, $R = -1$: (a, b) crack propagation zone; (c, d) final fracture zone.

configuration could be observed (Fig. 8b).

For metals with high stacking fault energy, such as Al, the extended dislocations were narrow, and cross-slip could occur by dislocation constriction [47–50]. Therefore, cell sub-structures were prone to form in the CGs, through the multiplication and interaction of dislocations during fatigue. In the UFGs, dislocation multiplication was very difficult due to the limitation of grain size and many of the newly formed dislocations would disappear at the grain boundaries, so the grain interiors were relatively clean, and no obvious dislocation configuration change was detected.

Fig. 9 shows the microstructure of the CNT/7055Al specimen

after fatigue under $\sigma_{max} = 450$ MPa and $R = -1$. Under relatively high-stress tension-compression fatigue, a few dislocations appeared in the CGs (Fig. 9a) and many dislocations accumulated at the boundaries between CG bands and UFG zones (marked by yellow rectangles), while no obvious dislocation configuration was observed in the UFGs (Fig. 9b). The distribution of CNTs was the same as those before fatigue. Some CNTs were distributed at the UFG boundaries and hindered the growth of UFGs, as shown by the circle in Fig. 9c.

Fig. 10 shows the microstructure of the CNT/7055Al specimen after 10^7 cycles under $\sigma_{max} = 300$ MPa and $R = -1$. Under low-

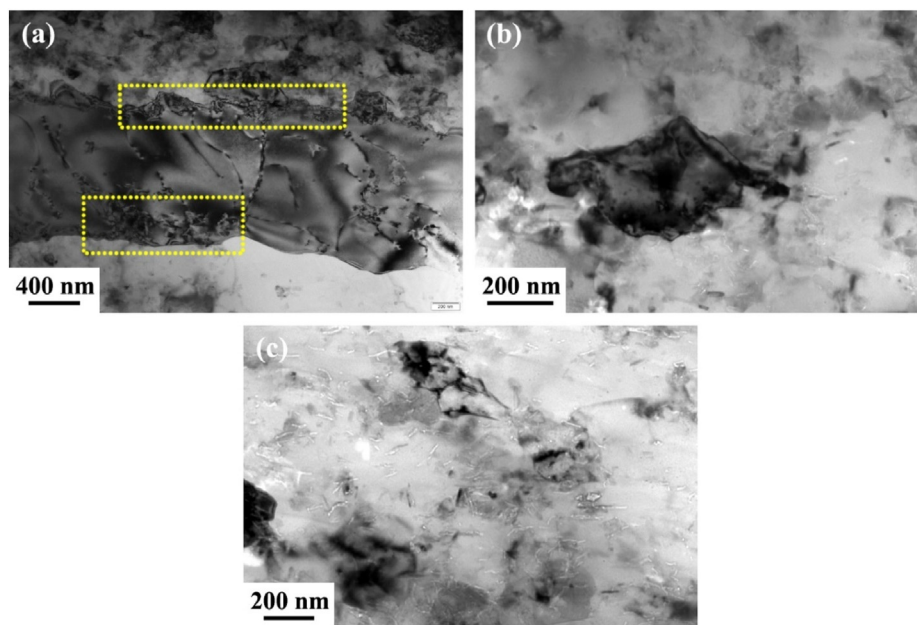


Fig. 7. Microstructure of different zones in CNT/7055Al specimens after fatigue under $\sigma_{max} = 600$ MPa, $R = 0.1$: (a) CG bands; (b, c) UFG zones (the yellow rectangles showing the dislocations at the grain boundaries). (A colour version of this figure can be viewed online.)

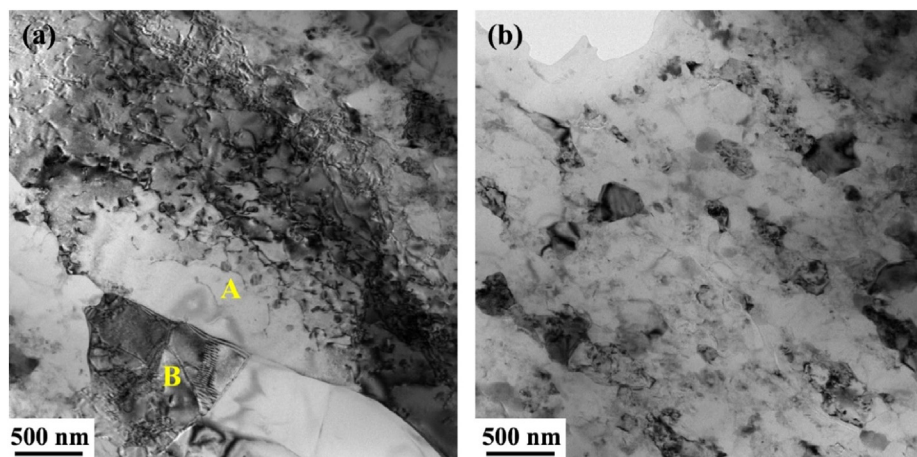


Fig. 8. Microstructure of different zones in the CNT/7055Al specimens after 10^7 cycles under $\sigma_{max} = 400$ MPa, $R = 0.1$: (a) CG bands; (b) UFG zones. (A colour version of this figure can be viewed online.)

stress tension-compression fatigue, a large number of cell structures were formed in the CG bands and many tangled dislocations could be observed at the boundaries between the UFG and CG zones as shown in the yellow rectangle in Fig. 10a. Furthermore, no obvious dislocation configuration was observed in the UFGs (Fig. 10b).

3.6. Surface morphology after fatigue

Fig. 11 shows the surface morphology of the CNT/7055Al specimens after fatigue. The images were taken at the sites far away from the fatigue fracture sites. After electropolishing, the CG and UFG zones could be clearly seen. Under the tension-tension fatigue, the cracks initiated in the CG bands (Fig. 11a). No cracks were observed in the UFG zones, indicating that the UFGs had resistance on the crack initiation. Under tension-compression fatigue, the cracks were observed in both CG and UFG zones (Fig. 11b). It can be

seen that some of the cracks inside the UFG zones initiated from the cracks in the CG bands, as shown by the yellow arrows. Further, some cracks inside the UFG zones initiated from the boundaries between CG bands and UFG zones, as shown by the black arrows, which was in accordance with the TEM image in Fig. 10a. At the location away from the CG band, nearly no cracks were detected, as shown in the yellow rectangle, which was due to that the UFGs had strong resistance to crack nucleation due to their high yield strength [51].

4. Discussion

4.1. Damage mechanism of CNT/7055Al composites

It is well known that the fatigue damage is closely related to dislocation slip in grains. Persistent slip band is the typical fatigue damage pattern for CG materials [38]. Shear band and grain

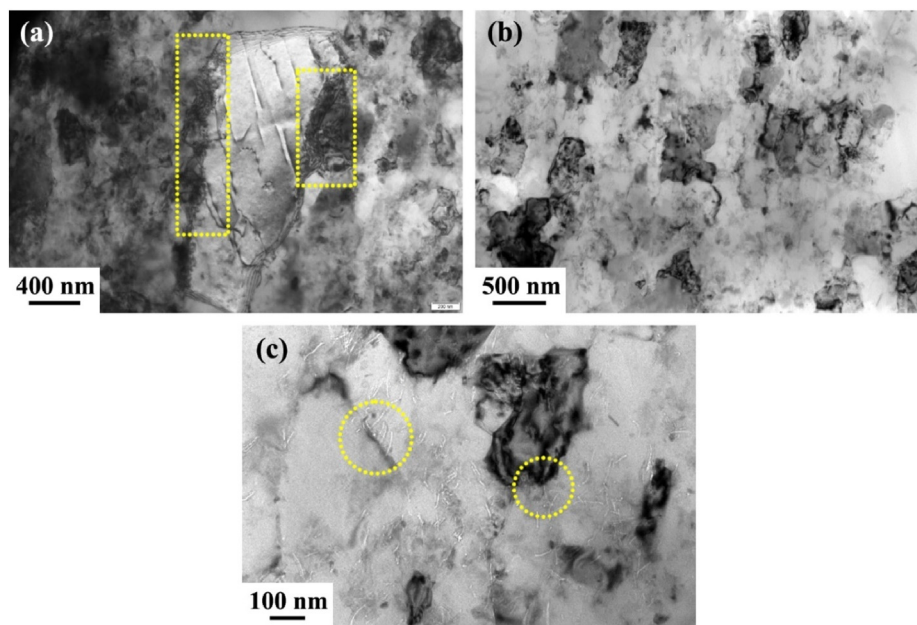


Fig. 9. Microstructure of different zones in the CNT/7055Al specimens after fatigue under $\sigma_{max} = 450$ MPa, $R = -1$: (a) CG bands; (b, c) UFG zones (the yellow rectangles and circles respectively showing the dislocations and CNTs near grain boundaries). (A colour version of this figure can be viewed online.)

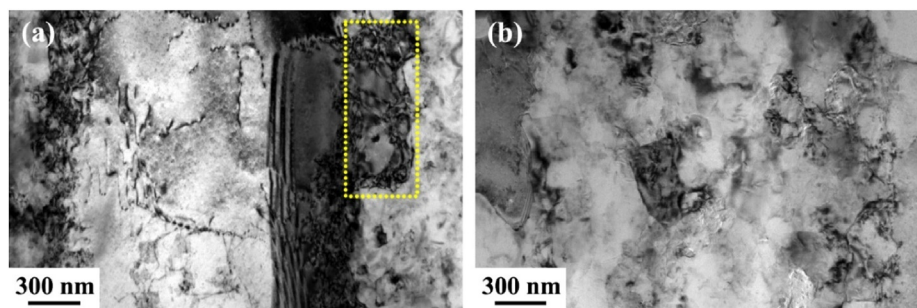


Fig. 10. Microstructure of different zones in CNT/7055Al specimens after 10^7 cycles under $\sigma_{max} = 300$ MPa, $R = -1$: (a) CG bands; (b) UFG zones (the yellow rectangle showing cell structures and tangled dislocations). (A colour version of this figure can be viewed online.)

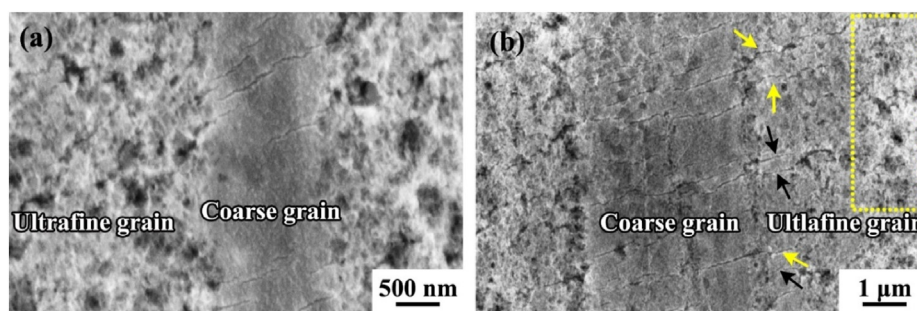


Fig. 11. Surface morphology of CNT/7055Al specimens after fatigue under (a) $\sigma_{max} = 500$ MPa, $R = 0.1$ and (b) $\sigma_{max} = 425$ MPa, $R = -1$ (Yellow and black arrows respectively denote the cracks initiated from the CGs and the boundaries, respectively. The loading direction is vertical). (A colour version of this figure can be viewed online.)

coarsening are the typical fatigue damage patterns for nano-grain or UFG materials [45,52]. Based on the observation of microstructure and surface morphology after fatigue, the fatigue damage process of CNT/7055Al composites could be understood as follows.

In the early stage of the cyclic deformation, dislocations were first formed in the CG bands (Figs. 7a and 9a). With the increase of cycle, the dislocation density in the CG bands increased and cell

structures were formed (Figs. 8a and 10a). Further, many dislocations formed at the boundaries between the CG bands and UFG zones (Figs. 7a, 8a and 9a and 10a). On the contrary, it is difficult to accommodate a large number of dislocations to activate the slip band due to the small grain size in the UFG zones. In addition, a small number of dislocations were easy to glide to the interface and annihilate, even if they initiated in the UFGs. So, dislocation

configuration was not obvious in the UFG zones (Figs. 8b and 10b). With the increase of dislocation density in CGs, cracks formed in the CGs (Fig. 11). That is why the preferential sites for fatigue damage in CNT/7055Al composites were both in the CG bands and under either the tension-tension or tension-compression fatigue.

In the tension-tension fatigue, the cracks in the CG bands were difficult to propagate to the UFG zones (Fig. 11a). However, in the tensile-compression fatigue, the cracks in the CG bands were more likely to propagate to the UFG zones, and the boundaries between the CG bands and UFG zones would also induce crack initiation in the UFG zones (Fig. 11b). As the cyclic deformation continued, the cracks propagated constantly, causing the fatigue fracture. That is also the reason why the $-b$ value of CNT/7055Al was even larger than that of the 7055Al alloy (Table 3). Therefore, the strain localization of CGs was the main damage mechanism of the CNT/7055Al composites.

4.2. The effect of stress ratio R on the fatigue strength

The FS of the CNT/7055Al composites under $R = 0.1$ and $R = -1$ were respectively 400 MPa and 300 MPa, indicating the performance of the composites in tension-tension fatigue was superior to that in tension-compression fatigue. This was attributed to the different stress amplitudes under two conditions. Previous studies have reported that slip deformation during fatigue was related to stress amplitude [53–55]. Liu et al. [53] reported that stress amplitude dominated the process of slip deformation. Chu et al. [54] and Shao et al. [55] demonstrated that only a single slip system was activated in a few grains under low stress amplitude, while multiple slip was activated in grains under high stress amplitude.

Fig. 12 shows the maximum stress and the corresponding stress amplitude under $R = 0.1$ and $R = -1$, respectively. As shown, the stress amplitude under tension-compression fatigue was much higher than that under tension-tension fatigue. As a result, more slip systems were activated and more cracks generated in the CG bands (Fig. 11). It is reported that UFGs had higher resistance to crack nucleation than CGs [42,45]. But once cracks formed, the crack growth rate of UFGs was much faster, which attributed to the poor crack propagation resistance of UFGs.

Further, the tension-compression fatigue led to the larger strain mismatch between UFG zones and CG bands (Figs. 8a and 9a),

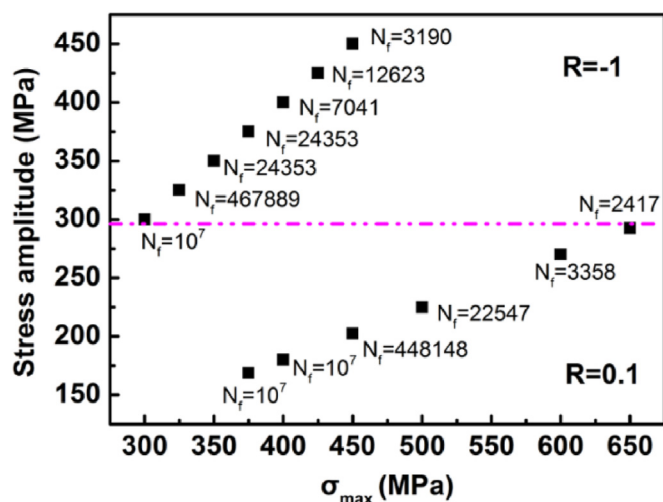


Fig. 12. The relationship between the maximum stress and stress amplitude of CNT/7055Al composites under $R = 0.1$ and $R = -1$ (N_f is the number of cycles). (A colour version of this figure can be viewed online.)

thereby resulting in higher stress concentration at the boundaries between CG bands and UFG zones. The huge stress concentration at the boundaries would accelerate the crack propagation from CG to UFG zones, or even induce crack initiation in UFG zones near the boundaries between CG bands and UFG zones (Fig. 11b). Therefore, the FS of CNT/7055Al composites under $R = -1$ was lower than that under $R = 0.1$.

4.3. The role of CNT under severe loading condition

Both CNT and carbon fiber were carbon materials with quasi 1D morphology, and thus carbon materials reinforced Al composites had some similar features during fatigue process [32,33,56,57], e.g., the carbon reinforcements could absorb the energy of crack propagation through the pulling-out and crack bridging mechanisms, thereby reducing the crack growth rate [58–60]. However, CNT in the CNT/Al composite had a much smaller aspect ratio and lower concentration compared with those of the carbon fiber in long carbon fiber/Al composite, which indicated that the main bearing part of CNT/Al composites was still Al matrix, while the main bearing part of long carbon fiber/Al composites was carbon fiber [61]. This means that the fatigue behavior between the above two composites might be a little different.

To examine the load transfer effects of the CNTs during fatigue, a Raman spectra test was performed on the composite specimens after fatigue (Fig. 13). It can be seen that the G peak of the as-received CNTs was at 1570 cm^{-1} , which was consistent with the peak position of the typical CNT. For the composite specimen without cycle deformation, the G peak shifted from 1570 cm^{-1} to 1615 cm^{-1} , resulting from that the CNTs were subjected to a large compressive stress due to the large thermal mismatch between CNTs and Al [62,63], which was consistent with our previous result [40].

After cyclic deformation, all the G peaks of the composite specimens shifted to the low Raman shift position. Under $R = 0.1$, the G peaks were slightly offset to the low Raman shift position, from 1615 cm^{-1} to around 1613 cm^{-1} . This was because the compressive stress on CNTs was relieved to a certain extent under the constant tension-tension fatigue. Under the severe condition ($R = -1$), the G peak of the composite specimens shifted to the low Raman shift position by a large margin. As the maximum stress was

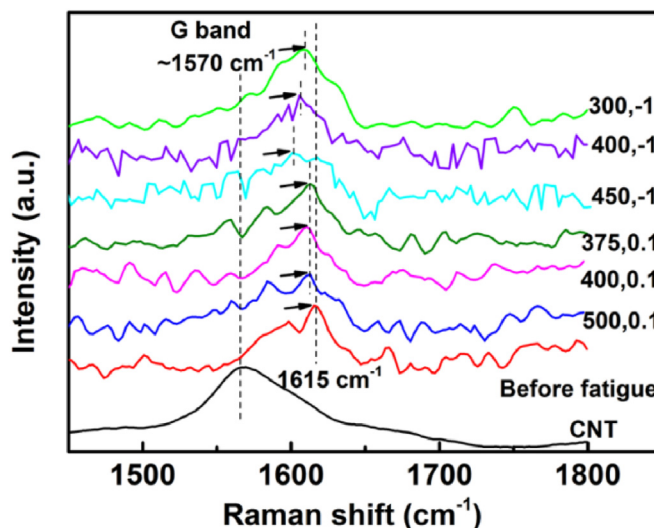


Fig. 13. Raman spectra of the as-received CNTs and CNT/7055Al composites before and after fatigue (500, 0.1 represents $\sigma_{max} = 500 \text{ MPa}$, $R = 0.1$, same labeling style for other specimens. The arrows denote the G band). (A colour version of this figure can be viewed online.)

450, 400 and 300 MPa, the G peaks shifted to 1600, 1606 and 1608 cm^{-1} , respectively. This was believed to result from the failure of the matrix in the UFG zones rich of CNTs, which greatly relieved the compressive stress on the CNTs.

That is, in the tension-tension fatigue, the CNT could still bear the load from the matrix, and improve the FS of the composites through the load transfer mechanism. On the contrary, in the tension-compression fatigue, higher stress concentration formed at the boundaries between the CG bands and UFG zones, which accelerated the damage in the UFG zones, thereby significantly reducing the load transfer efficiency from matrix to CNTs and failing to improve the FS of the composites. These results were in accordance with the CNT pulling-out situations under different fatigue conditions (Figs. 5 and 6).

4. Conclusions

The high-cycle fatigue behaviors of CNT/7055Al composites with bimodal structure were investigated under the stress ratio (R) of 0.1 and -1 , respectively. The damage mechanism of CNT/7055Al composites and the role of CNT under two cycle deformation conditions were analyzed.

- (1) The fatigue strength of CNT/7055Al composites under $R = 0.1$ was enhanced by CNTs due to the pulling-out mechanism and load transfer effect. However, the fatigue strength of CNT/7055Al composites was equivalent to that of unreinforced alloys under $R = -1$ owing to the failure of UFG zones rich of CNTs.
- (2) During the cyclic deformation of CNT/7055Al composites, the deformation mainly occurred in CG bands free of CNTs. Substructures (dislocation cells, tangles and subgrains) were observed in the CGs. Tangled dislocations were also detected at the boundaries between CG bands and UFG zones. However, no obvious dislocation configuration was observed in the UFGs due to the ultra-fine grain size, and no grain coarsening was identified because of the strong pinning effect of CNTs.
- (3) Strain localization of CG bands free of CNTs was the main damage mechanism of CNT/7055Al composites. In the tension-tension fatigue, the damage mainly occurred in the CG bands, while the damage occurred in both the CG bands free of CNTs and UFG zones rich of CNTs in the tension-compression fatigue, which attributed to the larger strain mismatch between the CG bands and UFG zones, resulting from the higher stress amplitude.

CRedit authorship contribution statement

S. Bi: Data curation, carried out the data collection, data analysis and manuscript writing. **Z.Y. Liu:** designed the experiment and revised the manuscript. **B.L. Xiao:** Data curation, participated in the design of the experiment and analysis of the experimental data. **P. Xue:** Data curation, helped to analyze the fatigue data. **D. Wang:** fabricated the composites. **Q.Z. Wang:** fabricated the composites. **D.R. Ni:** participated the microstructure analysis. **Z.Y. Ma:** Funding acquisition, revised the manuscript and provided the funding. All authors read and approved the final manuscript.

Declaration of competing interest

The authors declare that they have no known competing financial interests or personal relationships that could have appeared to influence the work reported in this paper.

Acknowledgement

This work was financially supported by the Key Research Program of Frontier Sciences, CAS (No. QYZDJ-SSW-JSC015), the National Key R&D Program of China (No. 2017YFB0703104), the National Natural Science Foundation of China (Nos. 51871215, 51931009, and 51871214) and the Youth Innovation Promotion Association CAS (No. 2020197).

References

- [1] K. Ma, Z.Y. Liu, S. Bi, X.X. Zhang, B.L. Xiao, Z.Y. Ma, Microstructure evolution and hot deformation behavior of carbon nanotube reinforced 2009Al composite with bimodal grain structure, *J. Mater. Sci. Technol.* 70 (2021) 73–82.
- [2] B. Chen, K. Kondoh, J.S. Li, M. Qian, Extraordinary reinforcing effect of carbon nanotubes in aluminium matrix composites assisted by in-situ alumina nanoparticles, *Composites, Part B* 183 (2020) 107691.
- [3] S. Saadallah, A. Cablé, S. Hamamda, K. Chetehouna, M. Sahli, A. Boubertakh, S. Revo, N. Gascoin, Structural and thermal characterization of multiwall carbon nanotubes (MWCNTs)/aluminum (Al) nanocomposites, *Composites, Part B* 151 (2018) 232–236.
- [4] S. Zhang, N. Nguyen, B. Leonhardt, C. Jolowsky, A. Hao, J.G. Park, R. Liang, Carbon-nanotube-based electrical conductors: fabrication, optimization, and applications, *Adv Electron Mater* 5 (6) (2019) 1800811.
- [5] S. Zhang, Y. Ma, L. Suresh, A. Hao, M. Bick, S.C. Tan, J. Chen, Carbon nanotube reinforced strong carbon matrix composites, *ACS Nano* 14 (8) (2020) 9282–9319.
- [6] S. Bi, Z.Y. Liu, B.H. Yu, G.N. Ma, L.H. Wu, B.L. Xiao, Z.Y. Ma, Superplastic deformation behavior of carbon nanotube reinforced 7055 Al alloy composites, *Mater. Sci. Eng., A* 797 (2020) 140263.
- [7] S. Bi, Z. Li, H. Sun, B. Song, Z. Liu, B. Xiao, Z. Ma, Microstructure and mechanical properties of carbon nanotubes reinforced 7055Al composites fabricated by high-energy ball milling and powder metallurgy processing, *Acta Metall. Sin.* 57 (1) (2021) 71–81.
- [8] K. Zhao, Z.Y. Liu, B.L. Xiao, D.R. Ni, Z.Y. Ma, Origin of insignificant strengthening effect of CNTs in T6-treated CNT/6061Al composites, *Acta Metall. Sin.* 31 (2) (2018) 134–142.
- [9] S.M.A.K. Mohammed, D.L. Chen, Carbon nanotube-reinforced aluminum matrix composites, *Adv. Eng. Mater.* 22 (4) (2019) 1901176.
- [10] H.J. Choi, B.H. Min, J.H. Shin, D.H. Bae, Strengthening in nanostructured 2024 aluminum alloy and its composites containing carbon nanotubes, *Composites, Part A* 42 (10) (2011) 1438–1444.
- [11] E.I. Salama, A. Abbas, A.M.K. Esawi, Preparation and properties of dual-matrix carbon nanotube-reinforced aluminum composites, *Composites, Part A* 99 (2017) 84–93.
- [12] X. Yang, T. Zou, C. Shi, E. Liu, C. He, N. Zhao, Effect of carbon nanotube (CNT) content on the properties of in-situ synthesis CNT reinforced Al composites, *Mater. Sci. Eng., A* 660 (2016) 11–18.
- [13] D.H. Nam, S.I. Cha, B.K. Lim, H.M. Park, D.S. Han, S.H. Hong, Synergistic strengthening by load transfer mechanism and grain refinement of CNT/Al–Cu composites, *Carbon* 50 (7) (2012) 2417–2423.
- [14] L. Shahrdami, A. Sedghi, M.H. Shaeri, Microstructure and mechanical properties of Al matrix nanocomposites reinforced by different amounts of CNT and SiCw, *Composites, Part B* 175 (2019) 107081.
- [15] S.E. Shin, Y.J. Ko, D.H. Bae, Mechanical and thermal properties of nanocarbon-reinforced aluminum matrix composites at elevated temperatures, *Composites, Part B* 106 (2016) 66–73.
- [16] R. Xu, Z. Tan, G. Fan, G. Ji, D.-B. Xiong, Q. Guo, Y. Su, Z. Li, D. Zhang, High-strength CNT/Al–Zn–Mg–Cu composites with improved ductility achieved by flake powder metallurgy via elemental alloying, *Composites, Part A* 111 (2018) 1–11.
- [17] R. Xu, Z. Tan, D. Xiong, G. Fan, Q. Guo, J. Zhang, Y. Su, Z. Li, D. Zhang, Balanced strength and ductility in CNT/Al composites achieved by flake powder metallurgy via shift-speed ball milling, *Composites, Part A* 96 (2017) 57–66.
- [18] B. Chen, K. Kondoh, H. Imai, J. Umeda, M. Takahashi, Simultaneously enhancing strength and ductility of carbon nanotube/aluminum composites by improving bonding conditions, *Scripta Mater.* 113 (2016) 158–162.
- [19] K. Ma, Z.Y. Liu, K. Liu, X.G. Chen, B.L. Xiao, Z.Y. Ma, Structure optimization for improving the strength and ductility of heterogeneous carbon nanotube/Al–Cu–Mg composites, *Carbon* 178 (2021) 190–201.
- [20] K. Ma, Z.Y. Liu, X.X. Zhang, B.L. Xiao, Z.Y. Ma, Hot deformation behavior and microstructure evolution of carbon nanotube/7055Al composite, *J. Alloys Compd.* 854 (2021) 157275.
- [21] M.M.H. Bastwros, A.M.K. Esawi, A. Wafi, Friction and wear behavior of Al–CNT composites, *Wear* 307 (1–2) (2013) 164–173.
- [22] N. Chawla, C. Andres, J.W. Jones, J.E. Allison, Effect of SiC volume fraction and particle size on the fatigue resistance of a 2080 Al/SiCp composite, *Metall. Mater. Trans.* 29 (11) (1998) 2843–2854.
- [23] N. Chawla, C. Andres, L.C. Davis, J.W. Jones, J.E. Allison, The interactive role of inclusions and SiC reinforcement on the high-cycle fatigue resistance of particle reinforced metal matrix composites, *Metall. Mater. Trans.* 31 (3A)

- (2000) 951–957.
- [24] N.E. Bekheet, R.M. Gadelrab, M.F. Salah, A.N. Abd El-Azim, The effects of aging on the hardness and fatigue behavior of 2024 Al alloy SiC composites, *Mater. Des.* 23 (2002) 153–159.
- [25] B.G. Park, A.G. Crosky, A.K. Hellier, High cycle fatigue behaviour of micro-sphere Al₂O₃-Al particulate metal matrix composites, *Composites, Part B* 39 (7–8) (2008) 1257–1269.
- [26] S.C. Tjong, G.S. Wang, Y.W. Mai, High cycle fatigue response of in-situ Al-based composites containing TiB₂ and Al₂O₃ submicron particles, *Compos. Sci. Technol.* 65 (10) (2005) 1537–1546.
- [27] J. Llorca, Fatigue of particle- and whisker-reinforced metal-matrix composites, *Prog. Mater. Sci.* 47 (3) (2002) 283–353.
- [28] D.P. Myriounis, T.E. Matikas, S.T. Hasan, Fatigue behaviour of SiC particulate-reinforced A359 aluminium matrix composites, *Strain* 48 (4) (2012) 333–341.
- [29] N. Chawla, Y.L. Shen, Mechanical behavior of particle reinforced metal matrix composites, *Adv. Eng. Mater.* 3 (6) (2001) 357–370.
- [30] C. Kaynak, S. Boylu, Effects of SiC particulates on the fatigue behaviour of an Al-alloy matrix composite, *Mater. Des.* 27 (9) (2006) 776–782.
- [31] J.N. Hall, J.W. Jones, A.K. Sachdev, Particle-size, volume fraction and matrix strength effects on fatigue behavior and particle fracture in 2124 Aluminim-SiC_p composites, *Mater. Sci. Eng., A* 183 (1–2) (1994) 69–80.
- [32] J.Z. Liao, M.J. Tan, E. Bayraktar, Tension-tension fatigue behaviour of carbon nanotube reinforced aluminium composites, *Mater. Sci. Forum* 765 (2013) 563–567.
- [33] S.E. Shin, D.H. Bae, Fatigue behavior of Al2024 alloy-matrix nanocomposites reinforced with multi-walled carbon nanotubes, *Composites, Part B* 134 (2018) 61–68.
- [34] J. Huang, J.E. Spowart, J.W. Jones, The role of microstructural variability on the very high-cycle fatigue behavior of discontinuously-reinforced aluminum metal matrix composites using ultrasonic fatigue, *Int. J. Fatig.* 32 (8) (2010) 1243–1254.
- [35] Z.Y. Liu, K. Ma, G.H. Fan, K. Zhao, J.F. Zhang, B.L. Xiao, Z.Y. Ma, Enhancement of the strength-ductility relationship for carbon nanotube/Al-Cu-Mg nanocomposites by material parameter optimisation, *Carbon* 157 (2020) 602–613.
- [36] K. Ma, Z.Y. Liu, B.S. Liu, B.L. Xiao, Z.Y. Ma, Improving ductility of bimodal carbon nanotube/2009Al composites by optimizing coarse grain microstructure via hot extrusion, *Composites, Part A* 140 (2021) 106198.
- [37] H. Mughrabi, H.W. Höppel, M. Kautz, Fatigue and microstructure of ultrafine-grained metals produced by severe plastic deformation, *Scripta Mater.* 51 (8) (2004) 807–812.
- [38] S.F. Toh, W.M. Rainforth, Fatigue of a nickel base superalloy with bimodal grain size, *Mater Sci Tech-lond* 12 (12) (1996) 1007–1014.
- [39] S. Bi, Z.Y. Liu, B.L. Xiao, Y.N. Zan, D. Wang, Q.Z. Wang, Z.Y. Ma, Enhancing strength-ductility synergy of carbon nanotube/7055Al composite via a texture design by hot-rolling, *Mater. Sci. Eng., A* 806 (2021) 140830.
- [40] S. Bi, B.L. Xiao, Z.H. Ji, B.S. Liu, Z.Y. Liu, Z.Y. Ma, Dispersion and damage of carbon nanotubes incarbon nanotube/7055Al composites during high-energy ball milling process, *Acta Metall. Sin.* 34 (2021) 196–204.
- [41] P.S. Pao, H.N. Jones, C.R. Feng, Fatigue crack growth and fracture toughness in bimodal Al 5083, in: I. Ovidko, C.S. Pande, R. Krishnamoorti, E. Lavernia, G. Skandan (Eds.), *Mechanical Properties of Nanostructured Materials and Nanocomposites*, Materials Research Society, Warrendale, 2004, pp. 17–22.
- [42] P. Cavaliere, Fatigue properties and crack behavior of ultra-fine and nanocrystalline pure metals, *Int. J. Fatig.* 31 (10) (2009) 1476–1489.
- [43] A.Y. Vinogradov, V.V. Stolyarov, S. Hashimoto, R.Z. Valiev, Cyclic behavior of ultrafine-grain titanium produced by severe plastic deformation, *Mater. Sci. Eng., A* 318 (1–2) (2001) 163–173.
- [44] H. Mughrabi, H.W. Höppel, Cyclic deformation and fatigue properties of very fine-grained metals and alloys, *Int. J. Fatig.* 32 (9) (2010) 1413–1427.
- [45] S. Malekjani, P.D. Hodgson, P. Cizek, T.B. Hilditch, Cyclic deformation response of ultrafine pure Al, *Acta Mater.* 59 (13) (2011) 5358–5367.
- [46] Z.Y. Liu, B.L. Xiao, W.G. Wang, Z.Y. Ma, Modelling of carbon nanotube dispersion and strengthening mechanisms in Al matrix composites prepared by high energy ball milling-powder metallurgy method, *Composites, Part A* 94 (2017) 189–198.
- [47] S. Bi, X.B. Yun, J.Y. Pei, Y. Zhao, Z.Y. Yan, X. Zhang, Microstructure evolution of Al-Sr master alloy during continuous extrusion, *T Nonferr Metal Soc* 27 (2) (2017) 305–311.
- [48] Y.N. Zan, Y.T. Zhou, H. Zhao, Z.Y. Liu, Q.Z. Wang, D. Wang, W.G. Wang, B.L. Xiao, Z.Y. Ma, Enhancing high-temperature strength of (B₄C+Al₂O₃)/Al designed for neutron absorbing materials by constructing lamellar structure, *Composites, Part B* 183 (2020) 107674.
- [49] Y.N. Zan, Q. Zhang, Y.T. Zhou, Z.Y. Liu, Q.Z. Wang, D. Wang, B.L. Xiao, W.C. Ren, Z.Y. Ma, Introducing graphene (reduced graphene oxide) into Al matrix composites for enhanced high-temperature strength, *Composites, Part B* 195 (2020) 108095.
- [50] Z.Y. Liu, L.H. Wang, Y.N. Zan, W.G. Wang, B.L. Xiao, D. Wang, Q.Z. Wang, D.R. Ni, Z.Y. Ma, Enhancing strengthening efficiency of graphene nano-sheets in aluminum matrix composite by improving interface bonding, *Composites, Part B* 199 (2020) 108268.
- [51] Y. Estrin, A. Vinogradov, Fatigue behaviour of light alloys with ultrafine grain structure produced by severe plastic deformation: an overview, *Int. J. Fatig.* 32 (6) (2010) 898–907.
- [52] A. Vinogradov, S. Hashimoto, Multiscale phenomena in fatigue of ultra-fine grain materials - an overview, *Mater T Jim* 42 (1) (2001) 74–84.
- [53] X. Liu, C. Sun, Y. Hong, Effects of stress ratio on high-cycle and very-high-cycle fatigue behavior of a Ti-6Al-4V alloy, *Mater. Sci. Eng., A* 622 (2015) 228–235.
- [54] R.Q. Chu, Z. Cai, S.X. Li, Z.G. Wang, Fatigue crack initiation and propagation in an alpha-iron polycrystal, *Mater. Sci. Eng., A* 313 (1–2) (2001) 64–68.
- [55] C.W. Shao, F. Shi, X.W. Li, Influence of cyclic stress amplitude on mechanisms of deformation of a high nitrogen austenitic stainless steel, *Mater. Sci. Eng., A* 667 (2016) 208–216.
- [56] N. Kumar, H.C. Chittappa, A.A.D. Mello, M.D. Kiran, Fatigue behavior of carbon fiber reinforced aluminum metal matrix composites, *Adv. Sci. Eng. Med.* 10 (2018) 463–466.
- [57] R. Valle, M.H. Vidal-Setif, D. Schuster, P. Le Vacon, Tensile and fatigue behavior of Al-based metal matrix composites reinforced with continuous carbon or A materials research society lumina fibers: Part II. Quasi-Unidirectional Composite Cross-Ply Laminates, *Metall. Mater. Trans.* 35A (2004) 3307–3317.
- [58] S.U. Khan, A. Munir, R. Hussain, J.-K. Kim, Fatigue damage behaviors of carbon fiber-reinforced epoxy composites containing nanoclay, *Compos. Sci. Technol.* 70 (14) (2010) 2077–2085.
- [59] S. Zhu, M. Mizuno, Y. Kagawa, Y. Mutoh, Monotonic tension, fatigue and creep behavior of SiC-fiber-reinforced SiC matrix composites: a review, *Compos. Sci. Technol.* 59 (1999) 833–851.
- [60] P. Cortes, W.J. Cantwell, The tensile and fatigue properties of carbon fiber-reinforced PEEK-titanium fiber-metal laminates, *J. Reinforc. Plast. Compos.* 23 (15) (2004) 1615–1623.
- [61] J.T. Xiong, H. Zhang, Y. Peng, J.L. Li, F.S. Zhang, Fabrication and characterization of plasma-sprayed carbon-fiber-reinforced aluminum composites, *J. Therm. Spray Technol.* 27 (4) (2018) 727–735.
- [62] O. Lourie, H.D. Wagner, Evaluation of Young's modulus of carbon nanotubes by micro-Raman spectroscopy, *J. Mater. Res.* 13 (9) (1998) 2418–2422.
- [63] C. Galiotis, D.N. Batchelder, Strain dependences of the first- and second-order Raman spectra of carbon fibres, *J. Mater. Sci.* 7 (1988) 545–547.